BIOCHEMISTRY

© Copyright 2004 by the American Chemical Society Volume 43, Number 44 November 9, 2004

Accelerated Publications

Ornithine Cyclodeaminase: Structure, Mechanism of Action, and Implications for the μ-Crystallin Family[†,‡]

Jessica L. Goodman,[§] Susan Wang,[∥] Shabnam Alam,[§] Frank J. Ruzicka,[∥] Perry A. Frey,[∥] and Joseph E. Wedekind*[,§]

Department of Biochemistry and Biophysics, University of Rochester School of Medicine and Dentistry, Box 712, Rochester, New York 14642, and Department of Biochemistry, University of Wisconsin, 1710 University Avenue, Madison, Wisconsin 53726

Received August 18, 2004; Revised Manuscript Received September 25, 2004

ABSTRACT: Ornithine cyclodeaminase catalyzes the conversion of L-ornithine to L-proline by an NAD^+-dependent hydride transfer reaction that culminates in ammonia elimination. Phylogenetic comparisons of amino acid sequences revealed that the enzyme belongs to the μ-crystallin protein family whose three-dimensional fold has not been reported. Here we describe the crystal structure of ornithine cyclodeaminase in complex with NADH, refined to 1.80 Å resolution. The enzyme consists of a homodimeric fold whose subunits comprise two functional regions: (i) a novel substrate-binding domain whose antiparallel β-strands form a 14-stranded barrel at the oligomeric interface and (ii) a canonical Rossmann fold that interacts with a single dinucleotide positioned for *re* hydride transfer. The adenosyl moiety of the cofactor resides in a solvent-exposed crevice on the protein surface and makes contact with a "domain-swapped"-like coil−helix module originating from the dyad-related molecule. Diffraction data were also collected to 1.60 Å resolution on crystals grown in the presence of L-ornithine. The structure revealed that the substrate carboxyl group interacts with the side chains of Arg45, Lys69, and Arg112. In addition, the ammonia leaving group hydrogen bonds to the side chain of Asp228 and the site of hydride transfer is 3.8 Å from C4 of the nicotinamide. The absence of an appropriately positioned water suggested that a previously proposed mechanism that calls for hydrolytic elimination of the imino intermediate must be reconsidered. A more parsimonious description of the chemical mechanism is proposed and discussed in relation to the structure and function of μ-crystallins.

In some clostridial strains, L-Orn[1] has been reported to serve as a hydrogen acceptor (*1*), an electron donor (*2*, *3*), or a fermentative substrate that is converted to L-Pro and ammonia (*4*). The stereospecific, irreversible conversion of L-Orn to L-Pro is accomplished by the enzyme ornithine cyclodeaminase (EC 4.3.1.12) (*5*), which has been identified in a modest number of soil and plant bacteria, and has been classified as a member of the μ-crystallin protein family on the basis of sequence similarity (∼45−47%) with proteins

[†] This work was supported by NIH Grants GM63162 (J.E.W.), GM62785 (B.M.G.), and GM30480 (P.A.F.). J.L.G. is a Miller Fellow for graduate study in Biophysics.

[‡] Protein Data Bank codes for reported structures: 1U7H for OCD−NADH and 1X7D for OCD−NADH−L-ornithine OCD.

* To whom correspondence should be addressed. Phone: (585) 273-4516. Fax: (585) 275-6007. E-mail: Joseph_Wedekind@URMC.Rochester.edu.

[§] University of Rochester School of Medicine and Dentistry.

[∥] University of Wisconsin.

[1] Abbreviations: L-Orn, L-ornithine; L-Pro, L-proline; OCD, ornithine cyclodeaminase; AlaDH, alanine dehydrogenase; MAD, multiwavelength anomalous diffraction; *Pp*, *Pseudomonas putida*; *Af*, *Archaeoglobus fulgidus*.

10.1021/bi048207i CCC: $27.50 © 2004 American Chemical Society
Published on Web 10/16/2004

localized in marsupial eye lens as well as human retina (*6*) and inner ear (*7*). Previously, the enzyme from *Clostridium sporogenes* was shown to be a dimer of identical subunits comprising a molecular mass of 80 kDa. The active enzyme was reported to bind one molecule of NAD^+ per dimer (*8*) with an apparent K_m of 6.1 μM (*5*). The dinucleotide cofactor was shown to be essential for catalytic activity and underwent transient reduction during the course of the reaction.

Investigation of the OCD mechanism identified loss of ammonia from the α-position of L-Orn, suggesting nucleophilic attack by its δ-amino group. The reaction has been suggested to proceed via hydride transfer leading to the formation of the intermediate 2-oxo-5-aminopentanoic acid, which subsequently cyclizes to form Δ^1-pyrroline-2-carboxylic acid (*8*). This stepwise process has been suggested to proceed via water-mediated hydrolysis of the imino intermediate due to the poor leaving group character of the α-amino moiety (*9*). The chemical mechanism is comparable to the oxidative deamination proposed for AlaDH, which leads to the formation of a keto acid and ammonia (*10*). However, the results of a crystallographic study that revealed AlaDH−pyruvate and AlaDH−NAD^+ binary complexes challenged the proposed mechanism (*11*). Specifically, the structural results were inconsistent with the stereochemistry assignments from solution measurements. However, the inability to crystallographically characterize the ternary enzyme−NAD^+−substrate or −product complexes has left the details of this, and comparable mechanisms, an open question.

To provide insight into the fold of the μ-crystallin protein family, as well as oxidative deamination mechanisms, we undertook a crystallographic study of OCD from *Pseudomonas putida*. Here we report the structure determination of OCD and its analysis in two ligand complexation states. The results are presented in the context of a revised mechanism for NAD^+-dependent ornithine cyclodeamination. Possible catalytic residues are described, as well as the amino acid signature sequences that differentiate OCD from other members of the μ-crystallin family. The results have functional implications for the crystallins derived from mammalian sources.

EXPERIMENTAL PROCEDURES

Protein Expression and Purification. *Escherichia coli* strains Rosetta (DE3) and B834(DE3) and vector pET-21a(+) were obtained from Novagen (Madison, WI). Chemicals and reagents were from Sigma-Aldrich (St. Louis, MO) or as described previously (*12*). Cloning and protein purification of the OCD gene were documented (*12*), but changes were made to produce the Se-Met protein. B834(DE3) cells were transformed with pET-21a-OCD. Minimal medium was made as described previously (*13*) except the final concentration of L-Se-Met was 0.3 mM (*14*). Starter cultures of 5 mL of LB broth and 100 μg/mL ampicillin were inoculated with single colonies of B834(DE3)-pET-21a-OCD and incubated for ~10 h at 37 °C with shaking. Starter cultures were used to inoculate 0.50 L of minimal medium containing 100 μg/mL ampicillin per 2 L flask; four cultures were incubated at 37 °C with vigorous shaking. At an OD_{600} of 1.2 (16 h), cells were induced with 0.5 mM IPTG, harvested by centrifugation after 3 h, and stored at −70 °C. Se-Met-labeled OCD was purified as the wild-type enzyme (*12*). Protein yields were ~10 mg/L for Se-Met OCD.

Crystallization. Se-Met-containing crystals were grown as described for the native protein (*12*) except for the following changes. Crystals grew in ~1 day by hanging-drop vapor diffusion from solutions of 0.1 M Na-MES (pH 6.25) and 40% MPD at 20 °C. Larger crystals (0.1 mm × 0.1 mm × 0.5 mm) were obtained under comparable conditions in 1−2 weeks at 4 °C. Because of their superior size, the latter crystals were selected for MAD phasing. Se-Met OCD was cocrystallized in the presence of 8 mM L-Orn at 20 °C as well. The habit of the Se-Met crystals did not change significantly in the presence and absence of substrate, nor were the unit cell dimensions affected by temperature changes.

X-ray Diffraction Experiments. Cryosolutions for L-Orn cocrystals contained 8 mM substrate. Crystals were cryoprotected in MPD (50%), flash-cooled to −190 °C, and tested for in-house diffraction as described previously (*12*). Crystals were stored subsequently in liquid nitrogen prior to synchrotron data collection. Diffraction data for the OCD−NADH structure were recorded at beamline X12C of the National Synchrotron Light Source (Upton, NY). Data for each wavelength (Table 1) were recorded at a distance of 16 cm on a Brandeis B4 CCD detector as 720 × 0.5° rotations with an exposure time of 5 s/frame. Intensities were reduced using the HKL2000 suite (*15*). Diffraction data for the Se-Met OCD−NADH−L-Orn complex (Table 1) were recorded at a distance of 15 cm on a Quantum 210 CCD detector (ADSC Inc.) at beamline A1 of the Cornell High Energy Synchrotron Source (CHESS) (Ithaca, NY) as 230 × 0.5° rotations with an exposure of 15 s/frame. Data were reduced using Crystal Clear (Rigaku/MSC).

Structure Determination and Refinement. The OCD−NADH structure was phased by a MAD experiment (Table 1). OCD from *P. putida* contains nine Met residues per polypeptide chain, and native crystals were shown to contain two polypeptide chains per asymmetric unit (*12*). Of the 18 Se sites, 16 were located with SOLVE version 2.03 (*16*). The initial data and experimental phases were of excellent quality to 1.80 Å resolution. The overall figure of merit was 0.72 with a quality score of 145.7, indicating the structure could have been built without density modification. However, phases were improved by 2-fold noncrystallographic symmetry averaging by use of RESOLVE and automated skeletonization with poly-Ala (*16*). This resulted in 540 Ala and 123 Gly residues of 700 possible residues. The density-modified structure factors were input to ARP/wARP for sequence docking and refinement by REFMAC (*17*). The resulting model contained 645 amino acids and 13 residues of poly-Gly at the C-terminus of chain A. The structure was completed by manual building in O (*18*). The structure of the OCD−NADH−L-Orn complex was determined by difference Fourier methods using the OCD−NADH structure as a starting model. Both structures were subjected to water picking and positional and individual *B*-factor refinement in CNS (*19*) with intervening rounds of manual adjustment. X-ray diffraction, phasing, and refinement statistics are reported in Table 1.

Absorption Measurements. Spectrophotometric measurements were recorded on crystals to corroborate the presence of NADH in refined structures. Eight crystals were removed from hanging drops and washed in synthetic mother liquor. All crystals were dissolved simultaneously in 0.50 mL of water, and readings were recorded. A significant peak at 340

Table 1: X-ray Data Collection and Refinement Statistics for Ornithine Cyclodeaminase

	Data Collection Statistics			
space group	$P2_12_12_1$			$P2_12_12_1$
unit cell (Å)	$a = 69.9$, $b = 78.6$, $c = 119.9$			$a = 69.8$, $b = 78.3$, $c = 119.9$
	OCD−NADH (MAD experiment)			
	inflection	peak	remote	OCD−NADH−L-Orn
wavelength (Å)	0.97946	0.97888	0.96114	0.9764
resolution (Å)	1.80−30	1.80−30	1.80−30	1.60−25
total no. of reflections	908255	751289	816359	374601
no. of unique reflections	62255	62209	62180	163396
completeness (%)	100 (100)[a]	100 (100)[a]	100 (100)[a]	97.0 (84.8)[a]
$\langle I\rangle/\sigma(I)$	42.8 (8.2)[a]	45.0 (10.1)[a]	39.4 (7.8)[a]	12.2 (3.8)[a]
R_{sym} (%)[b]	8.1 (37.2)[a]	8.0 (28.1)[a]	8.0 (37.5)[a]	4.6 (20.3)[a]

MAD Phasing Statistics for the OCD−NADH Complex (1.8−30 Å resolution)

	SOLVE	RESOLVE	ARP/wARP	CNS
figure of merit[c]	0.72 (0.49)[a]	0.77 (0.53)[a]	0.88 (0.64)[a]	0.92

Refinement Statistics for Complexes

	NADH as the ligand	NADH−L-Orn as the ligand
resolution range (Å)	1.80−25	1.60−25
no. of amino acids (average *B*)	681 (12.8 Å^2)	679 (13.7 Å^2)
no. of NADH molecules (average *B*)	2 (9.7 Å^2)	2 (10.4 Å^2)
no. of substrate molecules (average *B*)	none	2 L-Orn (13.9 Å^2)
no. of solvent molecules (average *B*)	751 (30.8 Å^2)	828 (32.8 Å^2)
no. of MPD/MES molecules (average *B*)	5 (36.0 Å^2)/0	6 (41.3 Å^2)/1 (42.3 Å^2)
no. of Na ions (average *B*)	2 (15.7 Å^2)	2 (13.7 Å^2)
σA coordinate error (Å)	0.10	0.15
anisotropy correction (Å^2)	$B_{11} = -0.63$, $B_{22} = 0.0$, $B_{33} = 0.64$	$B_{11} = -0.60$, $B_{22} = 0.75$, $B_{33} = -0.15$
R_{factor}/R_{free} (%)[d]	15.8/18.1	17.0/19.0
rms deviations from ideality		
bond lengths (Å)	0.005	0.005
bond angles (deg)	1.40	1.40
Ramachandran plot quality (%)[e]		
most favored	89.7	89.4
additionally allowed	10.3	10.6

[a] Data in parentheses are for the 1.80−1.86 or 1.60−1.65 Å resolution shell calculated on $|F_{hkl}|$ in the respective rows. [b] $R_{sym} = [\sum|I(h)_j - \langle I(h)\rangle|/\sum|I(h)_j|] \times 100$, where $I(h)_j$ is the intensity of the *j*th reflection of type *h* and $\langle I(h)\rangle$ is the average intensity of a reflection of type *h*. [c] Figure of merit = cos ϕ, where ϕ is the average error in the phase angle. [d] $R_{factor} = (\sum|F_{obs} - kF_{calc}|]/\sum|F_{obs}|) \times 100$, where *k* is a scale factor. R_{free} is defined as the R_{factor} calculated with 5% of the X-ray data selected randomly, and excluded from the refinement. [e] As defined by ProCheck (*33*).

nm whose magnitude diminished by serial dilution was observed.

Sequence Alignments. The sequence of *P. putida* OCD was compared to nine others identified by Psi-Blast (*20*). The GenBank accession numbers are NP_745670 (*P. putida*), AAN34071 (*Brucella suis*), ZP_00217643 (*Burkholderia cepacia*), AAO91222 (*Coxiella burnetii*), AAS13271 (*Treponema denticola*), BAA87813 (*Agrobacterium tumefaciens*), ZP_00193719 (*Mesorhizobium* sp. BNC1), NP_522044 (*Ralstonia solanacearum*), CAC49723 (*Sinorhizobium meliloti*), T03485 (*Rhodobacter capsulatus*), and AAB89583 (*Archaeoglobus fulgidus*). Subsequently, the μ-crystallins were added from *Macropus fulginosus* (western gray kangaroo, A46290) and *Homo sapiens* (AAB67600). Sequences were aligned with ClustalX (*21*) with secondary structure assignments added manually.

RESULTS

Structure Determination and Model Quality. The structure of *Pp*OCD was determined by MAD phasing (Table 1). The initial structure was refined to 1.80 Å resolution and employed subsequently to determine the cocrystal structure of an OCD−NADH−L-Orn complex that was refined to 1.60 Å resolution. Each refined, 700-amino acid structure exhibited continuous electron density for the entire main chain polypeptide from residue 2 to 342 (chain A) and from residue 1 to 340 (chain B) of the OCD−NADH complex and from residue 2 to 341 (chain A) and from residue 2 to 340 (chain B) of the ternary complex. The last eight disordered residues of the C-terminus are composed of the highly basic sequence ^{343}KRRIRRVA^{350}-COOH, which is not conserved among OCD sequences, suggesting these residues are not critical for enzymatic function. The high quality of each model is indicated by the low *R* values and temperature factors, and excellent stereochemistry (Table 1). Each structure had more than 99% of its residues in the allowed regions of a Ramachandran plot with coordinate errors of ≤0.15 Å [estimated by cross-validated σA plots as implemented in CNS (*19*)]. Representative simulated annealing omit electron density maps for the ligands NADH and L-Orn are provided (Figure 1).

Description of the Overall Fold. The structure of OCD comprises a dimer of identical subunits (Figure 2A), which corroborates previous sedimentation and size exclusion measurements on the enzyme from *C. sporogenes* (*22*). Each subunit comprises two domains that function in substrate binding and oligomerization (Figure 2A, cyan and purple domains) and cofactor binding (Figure 2A, blue and red

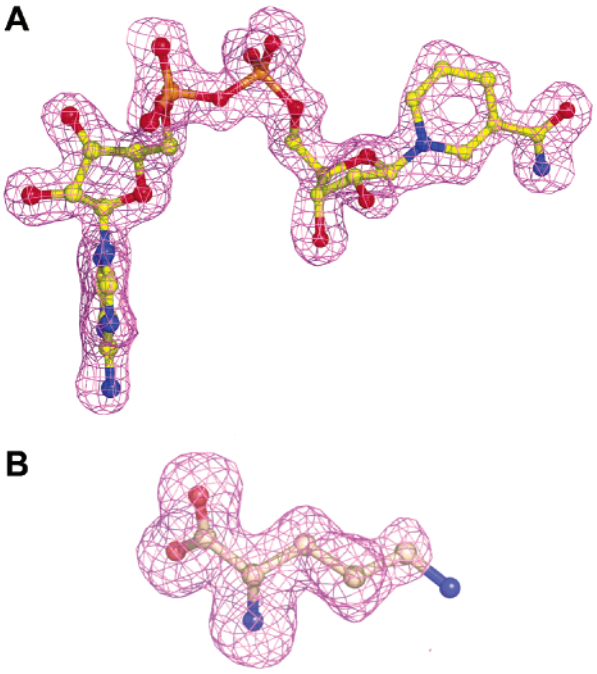

FIGURE 1: Representative $mF_o - DF_c$ simulated annealing omit electron density maps for *P. putida* OCD ligands. Models are depicted as ball-and-stick representations. Maps were contoured at 3.0σ. (A) Electron density for the omitted NADH cofactor calculated using data between 1.8 and 25 Å resolution. (B) Electron density for the omitted L-ornithine calculated using data between 1.6 and 25 Å resolution. This figure was generated with PyMol (*34*).

domains). A single dinucleotide binds per subunit via a Rossmann fold (Figure 2A), which differs from the previous stoichiometric assignment of one NAD^+ per dimer (*8*). The overall molecular dimensions of the OCD dimer are 50 Å × 85 Å × 30 Å, with the two longest dimensions oriented in the plane of Figure 2A. The structure is unusual in that a large concave surface exists at the subunit interface with a radius of 20 Å. The latter surface is formed by protuberances arising from extensions of the classical dinucleotide-binding domain (green and orange structures in Figure 2A), albeit the functional significance of these subdomains is unknown. A search for OCD-like folds using the Dali server (www.ebi.ac.uk/dali/) (*23*) revealed no homologous structures at the tertiary or quaternary levels. The most closely related protein fold is likely to be that of AlaDH from *A. fulgidus*, the sequnce of which was 37% identical to that of *Pp*OCD; however, its structure has not been reported. Interestingly, the gene for AlaDH was misannotated as an ornithine cyclodeaminase, although both *Pp*OCD and *Af*AlaDH belong to the μ-crystallin protein family based on sequence similarity (*24*). A comparison of the *Pp*OCD sequence with that of AlaDH and those of μ-crystallins is expected to reveal key differences that are necessary for enzyme classification and functional analysis.

*Dinucleotide-Binding Motif. Pp*OCD possesses an NAD^+-type Rossmann fold (*25*) embedded within the structure from residue 130 to 242 and from residue 288 to 293 (Figure 2A, red and blue domains). This classical domain comprises six parallel β-strands composed of a symmetrical repeat of a $\beta\alpha\beta\alpha\beta$ motif in which helices provide topological crossover elements (Figure 2B). The dinucleotide-binding fold is interrupted by a short subdomain (residues 243−287) that

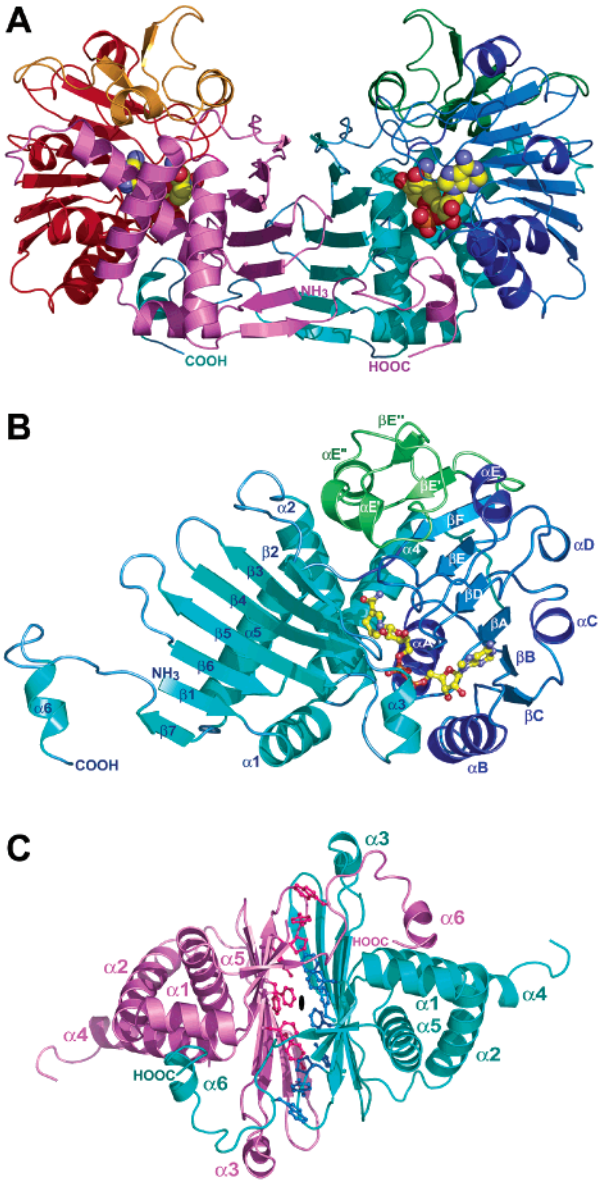

FIGURE 2: Ribbon diagrams for the OCD structure. (A) The dimeric structure looking down the 14-stranded β-barrel of the substrate-binding domain (violet and cyan). The dinucleotide-binding domain (red and dark blue) is drawn with bound NADH (space-filling model). (B) Bipartite OCD subunit with the substrate-binding domain (cyan) comprising $\beta1-\beta7$ and $\alpha1-\alpha6$ and "classical" dinucleotide-binding domain (dark blue) comprising $\beta A-\beta E$ and $\alpha A-\alpha E$ with inserted subdomains $\beta E'$ and $\beta E''$ and $\alpha E'$ and aE'' (green). NADH is drawn as a ball-and-stick model. (C) View of the oligomerization motif looking down the 2-fold axis (black oval). Hydrophobic residues contributed by each subunit are drawn as stick models. The view is rotated ~90° about the horizontal axis relative to panel A. This figure was generated with PyMol (*34*).

forms an extended β-sheet flanking strand βF. This extended structure has been labeled $\beta E'$ and $\beta E''$ (Figure 2B, green structure) to denote the discontinuity of the typical Rossmann topology. The additional structural features do not contribute directly to nucleotide or substrate binding, but rather abut the substrate-binding domain making van der Waals contacts between $\alpha E'$ and $\beta 2$ (Figure 2A). The latter strand harbors several key, active site residues, suggesting an important role for the subdomain in maintaining the functional enzyme.

To establish a precedent for the existence of other extended dinucleotide motifs, a Dali search was conducted (*23*). Two structures were identified with a seventh β-strand spatially equivalent to that of OCD βE′ (Figure 2B). However, these structures did not exhibit strand βE″, and their topologies were distinct from the subdomain insertion of OCD. The identified enzymes were (i) a human NAD^+-dependent transcriptional corepressor (*26*) (Z score = 10.9, rmsd = 4.9 Å for 160 aligned positions), which completes its βF strand prior to forming a seventh strand equivalent to βE′ of OCD, and (ii) cyanobacterial L-AlaDH (*11*) (Z score = 10.8, rmsd = 4.2 Å for 182 positions), which utilizes its seventh β-strand as a topological crossover element prior to completing its dinucleotide fold at βF; as such, it is analogous to OCD. The extra β-strand of AlaDH is antiparallel, in contrast to those of OCD and the corepressor. Finally, both of the identified enzymes exhibit a helix that is topologically and spatially equivalent to α4 of OCD, which precedes βA of the dinucleotide domain (Figure 2B). In total, the results demonstrate how topological changes at βF evolve to add new functionality, such as oligomerization or active site formation, while preserving the rudimentary dinucleotide-binding domain.

Substrate-Binding Domain. The role of the substrate-binding domain (Figure 2B, cyan domain) is to contribute residues essential for conversion of L-Orn to L-Pro in a manner that juxtaposes them closely to NAD^+. The domain architecture consists of a mixed α/β fold (Figure 2B) comprising (i) six β-strands and four α-helices from the N-terminal polypeptide (residues 1−129) and (ii) a helix−strand−helix motif (residues 294−350) at the C-terminus. The domain exhibits a $\beta7\beta1\beta6\beta5\beta4\beta3\beta2$ sheet topology (Figure 2B) buttressed on a single side by a four-helix bundle composed of α1, α2, α4, and α5 (Figure 2C). Helix α5 originates from the C-terminus of the protein and extends 27 Å across the face of the sheet (Figure 2B), culminating in strand β7, which completes the sheet by interacting with β1 at the N-terminus. The substrate-binding domain terminates in a notable structural feature. Specifically, helix α6, a 3_{10}-helix, appears "domain-swapped" because of its extensive incursion into the active site of the symmetry-related molecule (Figure 2A,B). Whether this interaction is a *bona fide* example of domain swapping has yet to be elucidated. Oligomerization results in a 14-stranded, closed β-barrel (Figure 2A,C). Each subunit contributes residues Phe4, Tyr66, Phe68, Tyr70, Phe88, Tyr98, Pro99, and Trp325 to the barrel interior (Figure 2C), making it a highly hydrophobic environment. The amount of surface area buried upon oligomerization is 7700 $Å^2$, which suggests a highly stable interface. An additional 250 $Å^2$ is buried by each coil−α6 segment. Although the latter interaction does not contribute significantly to dimer stability, it does contribute key residues to NAD^+ recognition and thereby distinguishes OCD sequences from others of the μ-crystallin family, which lack this sequence. A Dali search for structures comparable to Figure 2C yielded no results for either the monomeric or dimeric molecule.

Dinucleotide Binding. Each dinucleotide-binding domain of *Pp*OCD is occupied by a single molecule of NADH (Figure 2A). This observation is based upon the X-ray diffraction data, which are of sufficient quality to assign the nicotinamide ring as nonplanar (Figure 1A), and therefore reduced.

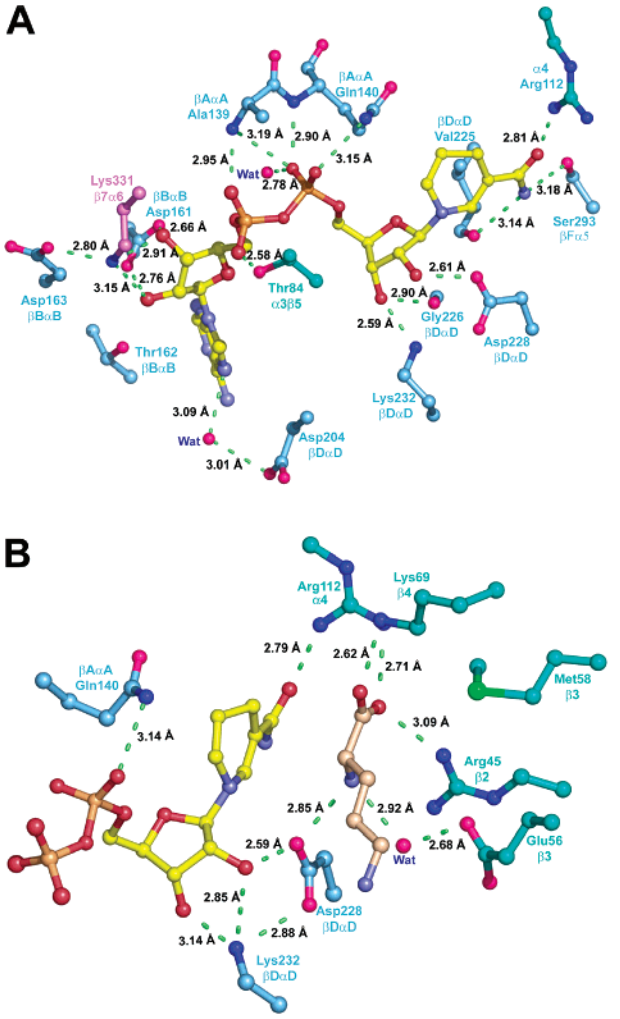

FIGURE 3: Diagrams of the dinucleotide- and substrate-binding sites. The color scheme and secondary structure are from Figure 2A. Interaction distances are the average of both subunits: (A) NADH-binding site and (B) L-ORN-binding site. This figure was generated with PyMol (*34*).

The presence of NADH is corroborated by significant absorption of dissolved crystals at 340 nm. No substrates or products were present in the crystallization medium of the initial OCD−NADH complex; however, spectrophotometric measurements conducted on the precrystallization protein indicated 20−25% was reduced. It is unclear whether the reduced form crystallized selectively, or if there is a mixed population of NAD^+ and NADH. The electron density maps are fully consistent with NADH, and atoms were modeled with full occupancy. The temperature factors of NADH atoms were comparable to those of the protein (Table 1).

The structural location of NADH is analogous to binding in other Rossmann folds (*27*). Detailed hydrogen bonding and van der Waals interactions are summarized in Figure 3A. The noted amino acids are conserved highly in other OCD sequences, as well as members of the μ-crystallin family (Figure 4). Protein interactions with the NADH can be divided into three regions of the cofactor. The adenosyl moiety is the only surface-exposed portion of the NADH, and no direct hydrogen bonds are made to the purine ring (Figure 3A). However, a water is observed to bridge N7 of the base and Asp204. The latter residue is a Ser in μ-crystallins (Figure 4), and hence, the interaction is unlikely

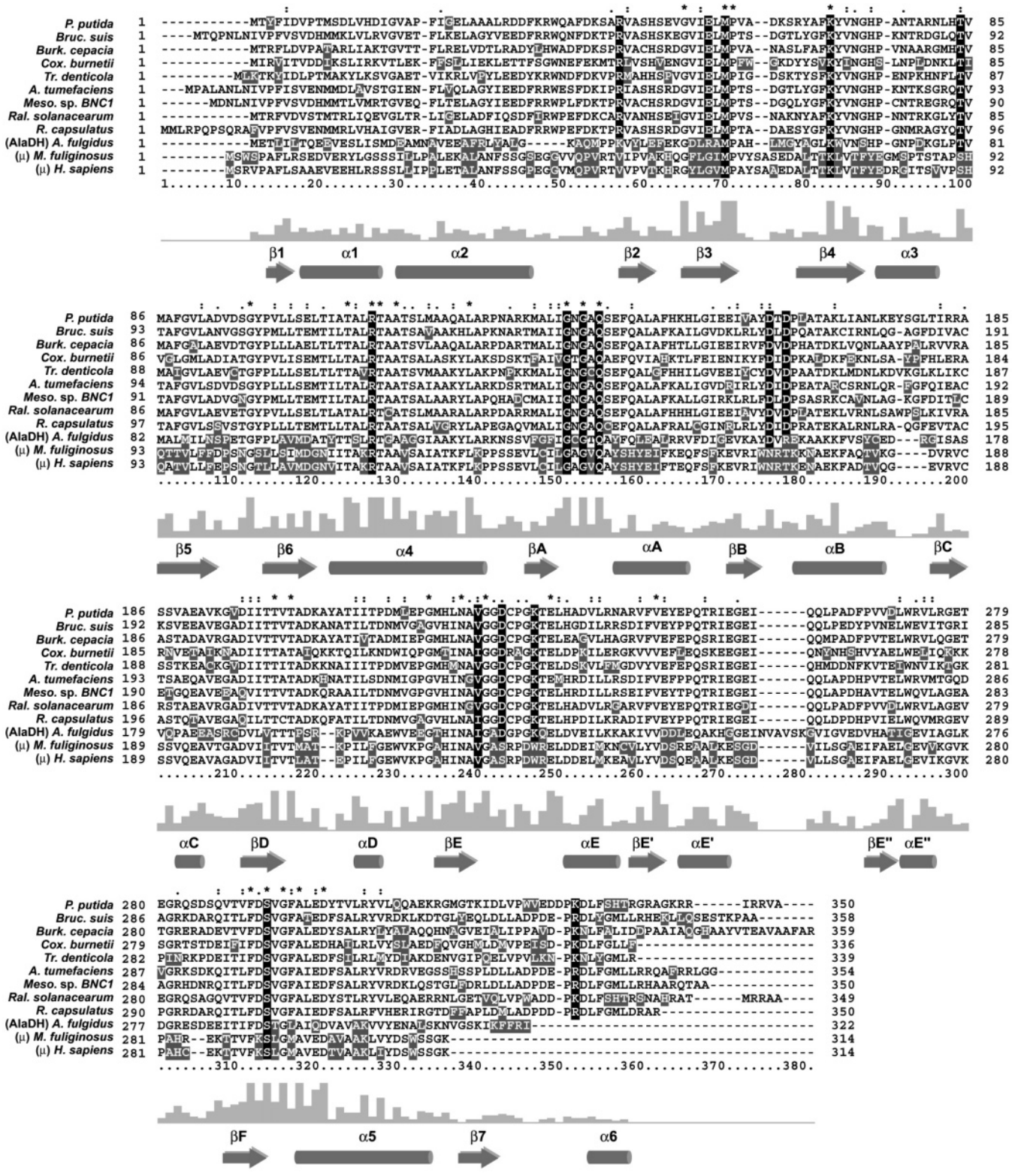

FIGURE 4: Amino acid alignments of OCD enzymes, AlaDH, and μ-crystallins (μ) with secondary structure assigned (below) on the basis of the OCD structure. Regions of identity (*), conservation (:), and similarity (.) are indicated above the alignments. Gray backgrounds denote nonconserved regions. Black backgrounds denote a high level of conservation of residues in the active site (depicted in Figure 3). The vertical histogram indicates varying sequence identity.

to be conserved. Thr162 makes a van der Waals contact with the six-membered heterocycle (Figure 3A), which is consistent with the observation that this residue is aliphatic in other OCD sequences (Figure 4). The 2′- and 3′-hydroxyl groups of the ribose moiety donate hydrogen bonds to the Asp161 carboxyl group (Figure 3A). Acidic residues have been observed in other dinucleotide-binding domains and often discriminate against $NADP^+$ binding (*27*). Because the Asp161 equivalent is Asn in μ-crystallins, and Thr162 is an Arg (Figure 4), it is likely that μ-crystallins evolved to bind $NADP^+$. This concept has been suggested previously on the basis of sequence comparisons and affinity chromatography

(*28*). Although all OCD sequences examined possess an Asp equivalent to position 161, these enzymes also exhibit a basic residue equivalent to Lys331. In the structure, the ϵ-amino group of Lys331 hydrogen bonds to the 2′-OH group of the adenine ribose, suggesting a means of binding a 2′-phosphate if the dinucleotide were $NADP^+$. However, it is unlikely that Asp161 could be displaced readily by a phosphate group for steric reasons. Additionally, Lys331 is restricted conformationally through a salt bridge interaction with Asp163 (Figure 3A), another conserved residue among OCD family members (Figure 4). These observations explain the preference for NAD^+ and are corroborated by the apparent K_m values of NAD^+ and $NADP^+$, which are 6.1 μM and 3 mM, respectively (*5*).

Like other dinucleotide folds, OCD binds the pyrophosphoryl moiety of the dinucleotide via a Gly rich loop located between βA and αA (Figures 2B and 4). However, whereas most phosphate-binding motifs have the sequence GxGxxG/A (where x is any residue), OCDs exhibit the sequence GxGxxS. This explains why previous studies dismissed the existence of canonical dinucleotide-binding sequences in OCD (*6*). A precedent for use of the GxGxxS sequence was established in studies of dihydropyrimidine dehydrogenase, which uses the latter motif in FAD^+ binding (*29*).

In *Pp*OCD, the nonbridging oxygens of pyrophosphate accept hydrogen bonds from both the substrate-binding and NADH-binding domains (Figure 3A). Thr84 of the substrate-binding domain contributes its OHγ group, whereas Ala139 and Gln140 of the Gly rich loop contribute their amide backbone hydrogens. Gln140 is conserved in all μ-crystallin sequences (Figure 4) most likely because it contributes its side chain amide group to pyrophosphate (Figure 3A). OCD, like other Rossmann folds, exhibits a conserved water that mediates a contact between O2N (Figure 3A) to the main chain amide of Gly138 of the Gly rich loop and the carbonyl oxygen of Val201 in strand βD (not shown). A similar interaction was documented in 77 of 102 high-resolution structures of dinucleotide-binding motifs (*30*).

In contrast to the adenosine moiety, the nicotinamide nucleoside exhibits numerous specific interactions. At ribose, the 2′- and 3′-OH groups donate hydrogen bonds to the side chain of Asp228 and the carbonyl oxygen of Gly226, respectively; the 3′-OH group also accepts a hydrogen bond from Lys232 (Figure 3A). These residues are conserved only among OCD and AlaDH sequences, whereas amino acids involved in nicotinamide ring interactions are highly conserved (Figure 4). Specifically, the nicotinamide moiety engages in hydrogen bond interactions with the side chains of Arg112 and Ser293, as well as the carbonyl oxygen of Val225, whose side chain makes van der Waals contact with the ring (Figure 3A). Overall, 9 of the 15 contacts to NADH are conserved among members of the μ-crystallin family with all but two, Thr84 and Arg112, originating from the dinucleotide-binding domain.

Interactions with Ornithine. Under the conditions of crystallization at pH 6.25, it is unlikely that there was appreciable catalytic activity because the pH optimum of the reaction is 8.0−8.2 (*5*). This is consistent with observations that L-Orn can be cocrystallized with the enzyme with negligible proline observed (Figure 1B). L-Orn binds in the active site in an extended conformation running parallel to the nicotinamide ring (Figure 3B). The main protein interactions that contribute to L-Orn recognition are a series of basic and acidic residues contributed by side chains from both substrate-binding and NADH-binding domains (Figure 3B, cyan vs light blue bonds). Specifically, the carboxylate moiety of L-Orn makes contacts with Arg45, Lys69, and Arg112. The α-amino group of L-Orn donates a hydrogen bond to the carboxylate group of Asp228. This interaction, along with salt bridge interactions to the carboxylate group, secures L-Orn in the active site and ensures that hydride transfer to the *re* face of nicotinamide occurs stereospecifically. The average distance between the C2 and C4 positions of the substrate and NADH is 3.8 Å. The modest number of interactions with L-Orn is consistent with the apparent K_m of 11 mM (*5*).

DISCUSSION

The structure of OCD from *P. putida* has been determined and refined to 1.80 Å resolution (Table 1). The global fold consists of a dimer whose oligomerization motif features a novel, robust 14-stranded β-barrel (Figure 2A). Each subunit comprises two domains that feature a substrate-binding motif coupled to a classical dinucleotide-binding domain (Figure 2B). The structure of OCD in complex with NADH and L-Orn firmly establishes the spatial locations and identities of amino acids involved in dinucleotide and substrate recognition. As such, it is now possible to evaluate previously postulated mechanisms for the NAD^+-dependent cyclodeamination mechanism.

Two distinct chemical mechanisms have been posited for OCD. In one proposal, the reaction was suggested to proceed via an imino intermediate that undergoes hydrolysis by water (*9*). This reaction is analogous to the oxidative deamination of L-amino acids to keto acids (*31*) and has been proposed for L-AlaDH and L-lactate DH (*11*). However, the OCD structure suggests that water-mediated attack is unlikely because there is insufficient accessibility to the C2 position of L-Orn. Although the structure clearly shows a water close to C2 (Figure 3B), this water bridges the side chain of Glu56 and the α-amino leaving group. In its current location, it would be unable to approach C2 due to steric interactions with the side chain of Arg45, which packs firmly against Met58. Therefore, it is unlikely that the active site will undergo significant conformational changes upon imino formation. Likewise, there is insufficient space to accommodate water between C2 and the nicotinamide ring.

An alternative mechanism has been suggested whereby water does not attack the imino intermediate (*32*). In light of the crystal structure, we favor this hypothesis and propose the following mechanism. L-Orn binds (Figure 3B), and hydride transfer to the *re* face of NAD^+ occurs, resulting in the imino substituent (Figure 5, intermediate 1). This process is facilitated by transfer of H^+ to the side chain of Asp228 (Figure 3B). Next, the δ-amino group directly attacks the C2 position of L-Orn (Figure 5, intermediate 2) in a manner that brings it close to the side chain of Glu56, consistent with the L-Pro stereochemistry. Although Glu56 may function as a proton acceptor (Figure 3B), the high pH optimum of the reaction (8.0−8.2) and the lack of candidate functional groups from the enzyme suggest that the macroscopic pK_a is consistent with deprotonation of the δ-amino group of L-Orn. The ensuing elimination of ammonia results in an

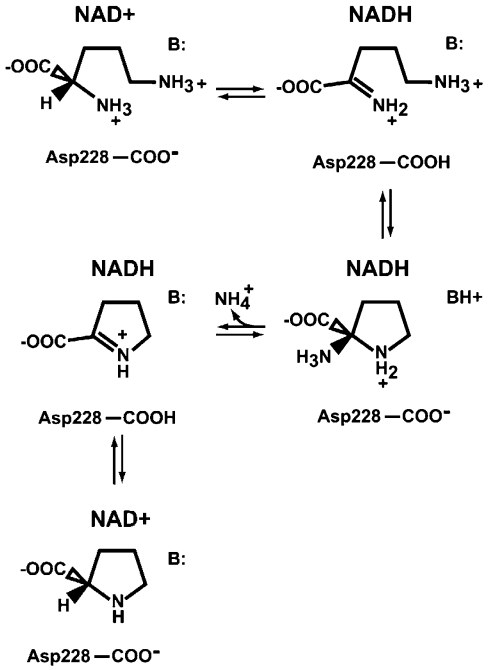

FIGURE 5: Possible catalytic mechanism for cyclodeamination of ornithine consistent with the structural data.

electrophilic C2 center (Figure 5, intermediate 3) that is susceptible to hydride transfer from NADH, yielding the L-Pro product. Further insight will require a structure of the OCD−NADH−L-Pro ternary complex.

Sequence alignments of *Pp*OCD with orthologous proteins indicated that active site residues identified in this study (Figure 3) are highly conserved (Figure 4). However, a sequence comparison between *Pp*OCD and the homologue from *A. fulgidus* revealed key differences. This is relevant because previous work established that the archaeal enzyme is not an OCD, but rather an AlaDH (*24*). Sequence differences include (i) the presence of Glu56 in *Pp*OCD versus Arg52 in *Af*AlaDH (Figure 3B); (ii) the consensus GxGxxS pyrophosphate-binding loop of *Pp*OCD, which is GxGxxA in *Af*AlaDH; (iii) the presence of two conserved acidic residues in the NAD^+ specificity pocket of *Pp*OCD (Figure 3A, Asp161 and Asp163), which are Asp157 and Arg159 in *Af*AlaDH, respectively; and (iv) the presence of an extended C-terminus in OCDs, which harbors a basic residue equivalent to Lys331 of *P. putida* (Figure 3A); neither *Af*AlaDH nor the μ-crystallins possess such an extended C-terminus. These amino acid differences should prove to be useful in the differential classification of OCDs versus AlaDHs of the μ-crystallin family.

In light of the OCD structure and the proposed mechanism, it is useful to consider the fold and function of μ-crystallins from eye-related sources. Proline is a significant osmolyte, and it has been proposed that the metabolic activity of lens crystallins has been co-opted to maintain lens transparency by regulation of osmolyte levels (*6*). Therefore, it was surprising when the μ-crystallin from western gray kangaroo (Figure 4) did not function as an OCD under conditions established for *Agrobacterium* (*6*). Although the lack of activity was attributed to post-mortum activity loss and nonoptimal assay conditions, the results of this study suggest that μ-crystallins bind $NADP^+$, but more importantly, they lack conserved catalytic residues necessary for binding L-Orn. Key differences include a change in residues Arg45 and Glu56 of OCDs to Val and Gly, respectively (Figures 3B and 4). Additionally, Asp228 of OCD, which interacts directly with the leaving α-amino group, is replaced with Ser. These observations strongly suggest the μ-crystallins do not support L-Orn cyclodeaminase activity. This comparison also implies that μ-crystallins are not competent to function as AlaDHs by analogy to the sequences of *A. fulgidus* (Figure 4). Whether the μ-crystallins exhibit any catalytic activity must await future studies. It is possible, however, that OCD was co-opted as a principal component of lens tissue simply for its robust structural properties and its propensity to form a highly refractive medium at high concentrations.

ACKNOWLEDGMENT

We thank Dr. Clara Kielkopf for helpful discussions and Dr. Howard Robinson for use of the mail-in data collection service at Brookhaven National Laboratory (Upton, NY). We thank the staff of CHESS for assistance in the use of beamline A1.

NOTE ADDED IN PROOF

While this paper was in review, the structure of the AlaDH−NAD^+ complex from *Archaeoglobus* at 2.3 Å resolution was published (*35*). The structure corroborates the overall fold of OCD presented here, but modeling studies with pyruvate suggested water-mediated attack of the substrate Cα, thereby demonstrating the chemical versatility of this protein family.

REFERENCES

1. Strickland, L. H. (1934) Studies in the metabolism of the strict anaerobes (genus *Clostridium*). I. The chemical reactions by which *Cl. sporogenes* obtains its energy, *Biochem. J. 28*, 1746−1759.
2. Stadtman, T. C. (1954) On the metabolism of an amino acid fermenting *Clostridium*, *J. Bacteriol. 67*, 314−320.
3. Stadtman, T. C., and White, F. H., Jr. (1954) Tracer studies on ornithine, lysine, and formate metabolism in an amino acid fermenting *Clostridium*, *J. Bacteriol. 67*, 651−657.
4. Mitruka, B. M., and Costilow, R. N. (1967) Arginine and ornithine catabolism by *Clostridium botulinum*, *J. Bacteriol. 93*, 295−301.
5. Costilow, R. N., and Laycock, L. (1971) Ornithine cyclase (deaminating). Purification of a protein that converts ornithine to proline and definition of the optimal assay conditions, *J. Biol. Chem. 246*, 6655−6660.
6. Kim, R. Y., Gasser, R., and Wistow, G. J. (1992) μ-Crystallin is a mammalian homologue of *Agrobacterium* ornithine cyclodeaminase and is expressed in human retina, *Proc. Natl. Acad. Sci. U.S.A. 89*, 9292−9296.
7. Abe, S., Katagiri, T., Saito-Hisaminato, A., Usami, S., Inoue, Y., Tsunoda, T., and Nakamura, Y. (2003) Identification of CRYM as a candidate responsible for nonsyndromic deafness, through cDNA microarray analysis of human cochlear and vestibular tissues, *Am. J. Hum. Genet. 72*, 73−82.
8. Muth, W. L., and Costilow, R. N. (1974) Ornithine cyclase (deaminating). III. Mechanism of the conversion of ornithine to proline, *J. Biol. Chem. 249*, 7463−7467.
9. Walsh, C. (1979) *Enzymatic Reaction Mechanisms*, W. H. Freeman and Co., San Francisco.
10. Grimshaw, C. E., Cook, P. F., and Cleland, W. W. (1981) Use of isotope effects and pH studies to determine the chemical mechanism of *Bacillus subtilis* L-alanine dehydrogenase, *Biochemistry 20*, 5655−5661.
11. Baker, P. J., Sawa, Y., Shibata, H., Sedelnikova, S. E., and Rice, D. W. (1998) Analysis of the structure and substrate binding of *Phormidium lapideum* alanine dehydrogenase, *Nat. Struct. Biol. 5*, 561−567.

12. Alam, S., Wang, S. C., Ruzicka, F. J., Frey, P. A., and Wedekind, J. E. (2004) Crystallization and X-ray diffraction analysis of ornithine cyclodeaminase from *Pseudomonas putida*, *Acta Crystallogr. D60*, 941−944.
13. Sambrook, J., Fritsch, E. F., and Maniatis, T. (1989) *Molecular Cloning*: *A Laboratory Manual*, Cold Spring Harbor Laboratory Press, Plainview, NY.
14. Budisa, N., Steipe, B., Demange, P., Eckerskorn, C., Kellermann, J., and Huber, R. (1995) High-level biosynthetic substitution of methionine in proteins by its analogs 2-aminohexanoic acid, selenomethionine, telluromethionine and ethionine in *Escherichia coli*, *Eur. J. Biochem. 230*, 788−796.
15. Otwinowski, Z., and Minor, W. (1997) Processing of X-ray Diffraction Data Collected in Oscillation Mode, *Methods Enzymol. 276*, 307−326.
16. Terwilliger, T. C. (2002) Automated structure solution, density modification and model building, *Acta Crystallogr. D58*, 1937−1940.
17. Perrakis, A., Morris, R., and Lamzin, V. S. (1999) Automated protein model building combined with iterative structure refinement, *Nat. Struct. Biol. 6*, 458−463.
18. Jones, T. A., Zou, J. Y., Cowan, S. W., and Kjeldgaard, M. (1991) Improved methods for building protein models in electron density maps and the location of errors in these models, *Acta Crystallogr. A47*, 110−119.
19. Brünger, A. T., Adams, P. D., Clore, G. M., DeLano, W. L., Gros, P., Grosse-Kunstleve, R. W., Jiang, J. S., Kuszewski, J., Nilges, M., Pannu, N. S., Read, R. J., Rice, L. M., Simonson, T., and Warren, G. L. (1998) Crystallography and NMR system: A new software suite for macromolecular structure determination, *Acta Crystallogr. D54*, 905−921.
20. Altschul, S. F., Madden, T. L., Schaffer, A. A., Zhang, J., Zhang, Z., Miller, W., and Lipman, D. J. (1997) Gapped BLAST and PSI-BLAST: a new generation of protein database search programs, *Nucleic Acids Res. 25*, 3389−3402.
21. Thompson, J. D., Gibson, T. J., Plewniak, F., Jeanmougin, F., and Higgins, D. G. (1997) The CLUSTAL_X windows interface: flexible strategies for multiple sequence alignment aided by quality analysis tools, *Nucleic Acids Res. 25*, 4876−4882.
22. Muth, W. L., and Costilow, R. N. (1974) Ornithine cyclase (deaminating). II. Properties of the homogeneous enzyme, *J. Biol. Chem. 249*, 7457−7462.
23. Holm, L., and Sander, C. (1999) Protein folds and families: sequence and structure alignments, *Nucleic Acids Res. 27*, 244−247.
24. Smith, N., Mayhew, M., Robinson, H., Heroux, A., Charlton, D., Holden, M. J., and Gallagher, D. T. (2003) Crystallization and phasing of alanine dehydrogenase from *Archaeoglobus fulgidus*, *Acta Crystallogr. D59*, 2328−2331.
25. Rossmann, M. G., Moras, D., and Olsen, K. W. (1974) Chemical and biological evolution of nucleotide-binding protein, *Nature 250*, 194−199.
26. Kumar, V., Carlson, J. E., Ohgi, K. A., Edwards, T. A., Rose, D. W., Escalante, C. R., Rosenfeld, M. G., and Aggarwal, A. K. (2002) Transcription corepressor CtBP is an NAD^+-regulated dehydrogenase, *Mol. Cell 10*, 857−869.
27. Branden, C., and Tooze, J. (1991) in *Introduction to Protein Structure*, pp 141−159, Garland Publishing, New York.
28. Segovia, L., Horwitz, J., Gasser, R., and Wistow, G. (1997) Two roles for μ-crystallin: a lens structural protein in diurnal marsupials and a possible enzyme in mammalian retinas, *Mol. Vision 3*, 9.
29. Dobritzsch, D., Schneider, G., Schnackerz, K. D., and Lindqvist, Y. (2001) Crystal structure of dihydropyrimidine dehydrogenase, a major determinant of the pharmacokinetics of the anti-cancer drug 5-fluorouracil, *EMBO J. 20*, 650−660.
30. Bottoms, C. A., Smith, P. E., and Tanner, J. J. (2002) A structurally conserved water molecule in Rossmann dinucleotide-binding domains, *Protein Sci. 11*, 2125−2137.
31. Grimshaw, C. E., and Cleland, W. W. (1981) Kinetic mechanism of *Bacillus subtilis* L-alanine dehydrogenase, *Biochemistry 20*, 5650−5655.
32. Graupner, M., and White, R. H. (2001) *Methanococcus jannaschii* generates L-proline by cyclization of L-ornithine, *J. Bacteriol. 183*, 5203−5205.
33. Laskowski, R. A., MacArthur, M. W., Moss, D. S., and Thornton, J. M. (1993) PROCHECK: a program to check the stereochemical quality of protein structures, *J. Appl. Crystallogr. 26*, 283−291.
34. DeLano, W. L. (2002) *The PyMOL Molecular Graphics System*, DeLano Scientific, San Carlos, CA.
35. Gallagher, D. T., Monbuoquette, H. G., Schröder, I., Robinson, H., Holden, M. J., and Smith, N. N. (2004) Structure of alanine dehydrogenase from *Archaeoglobus*: Active site analysis and relation to bacterial cyclodeaminases and mammalian μ-crystallin, *J. Mol. Biol. 342*, 119−130.

BI048207I